Research Article | Vol. 27, No. 18 / 2 September 2019 / Optics Express 24866
Optics EXPRESS

Hybrid graphene metasurface for near-infrared absorbers

MD. MAHFUZUR RAHMAN,[1,2] AIKIFA RAZA,[2] HAMMAD YOUNES,[2] AMAL ALGHAFERI,[2] MATTEO CHIESA,[2,3] AND JINYOU LU[2,*]

[1]*Department of Industrial and Production Engineering (IPE), Military Institute of Science and Technology (MIST), Mirpur, Dhaka, Bangladesh*
[2]*Laboratory for Energy and Nano Science, Department of Mechanical and Materials Engineering, Khalifa University, Abu Dhabi, United Arab Emirates*
[3]*Arctic Renewable Energy Center (ARC), Department of Physics and Technology, UiT The Arctic University of Norway, Norway*
[*]*chun.lu@ku.ac.ae*

Abstract: We experimentally demonstrated an amorphous graphene-based metasurface yielding near-infrared super absorber characteristic. The structure is obtained by alternatively combining magnetron-sputtering deposition and graphene transfer coating fabrication techniques. The thickness constraint of the physical vapor–deposited amorphous metallic layer is unlocked and as a result, the as-fabricated graphene-based metasurface absorber achieves near-perfect absorption in the near-infrared region with an ultra-broad spectral bandwidth of 3.0 μm. Our experimental characterization and theoretical analysis further point out that the strong light-matter interaction observed is caused by localized surface plasmon resonance of the metal film's particle-like surface morphology. In addition to the enhanced light absorption characteristics, such an amorphous metasurface can be used for surface-enhanced Raman scattering applications. Meanwhile, the proposed graphene-based metasurface relies solely on CMOS-compatible, low cost and large-area processing, which can be flexibly scaled up for mass production.

1. Introduction

In recent times, there have been a growing interest in perfect absorbers or so-called super absorbers, which fully absorb electromagnetic radiations at specific wavelengths ranging from the visible to infrared regions, owing to their potential in enhancing performances in solar energy conversion [1,2], thermal imaging [3], thermophotovaltaics [4], and sensors [5]. Traditionally, such perfect absorbers are designed with multi-layered coatings [6,7], which allow impedance matching between the refractive index of air and the effective optical constants of the absorbers. Therefore, most of the intensity of incident light is absorbed and a near-zero percentage of light is reflected back to the air. However, multilayer coatings lead to thicker optical devices, and thus the current trends for realizing such perfect absorbers resort to so-called metasurfaces, which are nanostructures with controlled geometry and periodicity that are easy to implement into downscaled optical components.

With the flexibility of current state-of-the-art nanofabrication approaches, recent developments of metasurfaces [8] can yield near perfect light absorption in the visible [9], near-infrared [10], mid-infrared [11], and far-infrared [12] regions. Among these perfect absorbers, the three-layer configuration is designed with a metasurface on the top, a dielectric spacer in the middle, and a metallic reflector at the bottom, which is analogous to so-called Salisbury screen [13]. However, these metasurface-based absorbers are usually fabricated using sophisticated lithography techniques, such as E-beam lithography [14], laser interference lithography [15], self-assembly [16], and nanoimprint lithography [17], which limits large-scale mass production.

#362110 https://doi.org/10.1364/OE.27.024866
Journal © 2019 Received 11 Mar 2019; revised 17 Jul 2019; accepted 6 Aug 2019; published 19 Aug 2019

Optics EXPRESS

Revelations from the outstanding properties of these materials motivated the search for alternative materials with similar functionalities but less complicated fabrication requirements. Graphene, which is two-dimensional sheet of sp^2-hybridized carbon atoms arranged in a hexagonal lattice, surfaced as an extraordinary candidate due to its exceptional electrical, mechanical, and optical properties [18–20]. A number of approaches have been proposed to enhance the light absorption in optical devices by coupling structured graphene with dielectric or metallic resonant structures [21–23], which offers great opportunities and flexibility for light manipulation. In addition, physical vapor deposited amorphous metasurfaces [24,25] started to draw attention owing to their relatively simple fabrication pathways. Absorber coatings conceived to achieve near perfect absorption at specific wavelength range have been demonstrated by integrating vapor deposited amorphous metamaterials, such as metallic amorphous metasurfaces [26,27] dielectric/metal [28–30], semiconductor/metal [24], and metal/metal alloys nanocomposite films [31]. Among these coatings, metallic amorphous metasurfaces are fabricated by sputtering [26], thermal dewetting [32], spin coating [33] approaches, which are straightforward to implement into conventional clean room fabrication processes. However, the optical properties of metallic amorphous metasurfaces are constrained by their surface morphology related to the coating thickness, which is cumbersome to tune with the necessary resolution for different applications.

Here, we report a facile approach to turn amorphous metallic metasurface into a 3D amorphous film comprising of randomly distributed metallic nanoparticles obtained by combining sputtering deposition and graphene transfer coating [34]. The monolayer graphene fabricated by chemical vapor deposition [19,35] is used as a separation layer at the interface between metasurfaces, which offers additional degree of freedom for controlling the thickness of the metasurface. By alternatively coating silver amorphous metasurface and monolayer graphene, a super broadband near-infrared absorber consisting of integrated graphene with plasmonic metasurfaces achieve near perfect absorption around 2 μm with an ultra-broad bandwidth of 3.0 μm. In addition to the light absorption enhancement, such metasurfaces have a potential in surface enhanced Raman scattering applications, as indicated by characterizing sandwiched graphene with metasurfaces.

2. Experimental

2.1. Silver thin film deposition with sputtering approach

Silver thin films were fabricated with a commercial magnetron sputtering equipment (AJA international, Inc.). Prior to the deposition process, the sputtering chamber was evacuated to a pressure lower than 3×10^{-7} Torr. DC power (7 W) was supplied to the Ag target (99.99%, 3 in. diameter). The process was performed in an argon plasma environment at a pressure of 4 mTorr.

2.2. CVD-grown graphene on copper and the transfer process

Graphene films were synthesized on copper foils via cold wall CVD process (The AIXTRON Black Magic CVD furnace). As received copper foils (0.025 mm (0.001 in) thick, annealed, uncoated, 99.8% (metals basis), Alfa Aesar) were cleaned with 15 mins of sonication in acetone followed by 15 mins of sonication in isopropyl alcohol (IPA) prior to the CVD process. The cold wall CVD chamber consists of top and bottom heater where bottom heater (Tbott) and top heater temperatures (Ttop) were first raised up to 1070 °C and 800-950 °C respectively in the presence of flowing nitrogen (N_2) and hydrogen (H_2) gases. Then, methane (CH_4) is used as the carbon precursor with the flow rate of 7 sccm (standard cubic centimeter per minute). The growth time was 50 minutes to grow a continuous layer of monolayer graphene. Finally, the chamber was cooled down under N_2 environment to prevent the oxidation of the copper surface. As-grown graphene samples were characterized by Raman spectroscopy, which indicates monolayer graphene deposition. For the clean transfer of graphene, Poly(methyl methacrylate) (PMMA) solution was spin coated on to the CVD-grown graphene samples at 2000 rpm for

Optics EXPRESS

90 seconds and then cured at 80°C for 3 mins. Finally, the backside graphene was removed by oxygen plasma etching for 30 s where oxygen flow rate was about 10 sccm prior to etching copper using 2 wt% aqueous ammonium persulphate solution. After transfer, PMMA was removed by dilution in hot acetone (50°C). We have included the discussion on achieving clean graphene coating in Appendix A.

2.3. Structural and optical characterization

The top morphology of silver thin films and the metasurface-based absorber was characterized by SEM (Nova NanoSEM 650). Based on the SEM images, structural characteristic including film thickness, interparticle spacing, and the average size of the Ag particles were evaluated. The UV-vis absorption spectra were recorded with a Perkin-Elmer Model Scan LAMBDA 1050 UV/Vis/NIR Spectrophotometer.

2.4. Finite-difference time domain method

A commercial-grade simulator [36] based on the FDTD method [37] was used to perform the calculations. The 10 nm-thick silver metasurface is simulated as the silver with measured surface morphology from atomic force microscopy characterization. The dielectric function of granular Ag nanoparticles was taken from the Lorentz-Drude model which was fitted with Palik data [38]. Periodic boundary conditions were assigned in the xy-lateral directions with lateral cross section of 100×100 nm^2. The mesh size used in the FDTD domain in this work is 0.25 nm.

3. Results and discussions

We started by systematic study of silver thin films with different thickness grown on silicon wafers using a magnetron sputtering (AJA Orion 300) technique. The optical properties and surface morphologies of as-fabricated silver thin films are characterized using spectroscopic ellipsometry and scanning electron microscopy, respectively. In Figs. 1(a)–1(b), the measured optical properties of silver thin films fitted from ellipsometry characterization show that as the film thickness is below approximately 10 nm, the silver layer shows dielectric-like behavior and is highly lossy in the visible and near-infrared regions owing to its particle-like surface morphology (clearly visible in Fig. 1(c). In this work, the particle-like non-continuous film with 10 nm thickness is referred to as the amorphous metasurface. As the film thickness becomes larger than 10 nm, the film moves towards a continuous structure with smooth morphology, as shown in Fig. 1(d). The smooth silver layer exhibits metallic-like and reflective optical properties, which is a behavior similar to that observed for bulk silver [38]. Finite-difference time domain (FDTD) method [37] is used to investigate the optical properties of the silver amorphous metasurfaces. By using atomic force microscopy, the surface morphology is obtained and inputted into our FDTD optical simulation domain, as indicated in Fig. 2(a). Details of the 3D FDTD simulation are included in the computational section. Our FDTD simulation results in Fig. 2(b) show that in a three-layer metasurface-insulator-metal configuration, the optical devices absorb light in the near-infrared and their absorption peak can be tuned by changing the SiO_2 spacer thickness. The absorption is achieved owing to the strong plasmonic interaction [39,40] in such a metallic amorphous metasurface, consisting of randomly distributed silver nanoparticles, as indicated by Fig. 2(c).

Furthermore, we perform analytical calculations using transfer matrix method (TMM) [41], to scrutinize the near-perfect optical constants for designing metasurface coating, where the layer placed above silica coated silver reflector is calculated, as shown in Fig. 7 of Appendix B. Our study shows the sputtered silver films with 10 nm thickness has similar optical properties, as those required for achieving perfect absorption predicted by TMM calculations. By inputting the fitted optical constants of 10 nm-thick metasurface in the TMM calculations as a top layer, the results show that by increasing the spacer layer thickness, the absorptance is decreased and its

Optics EXPRESS

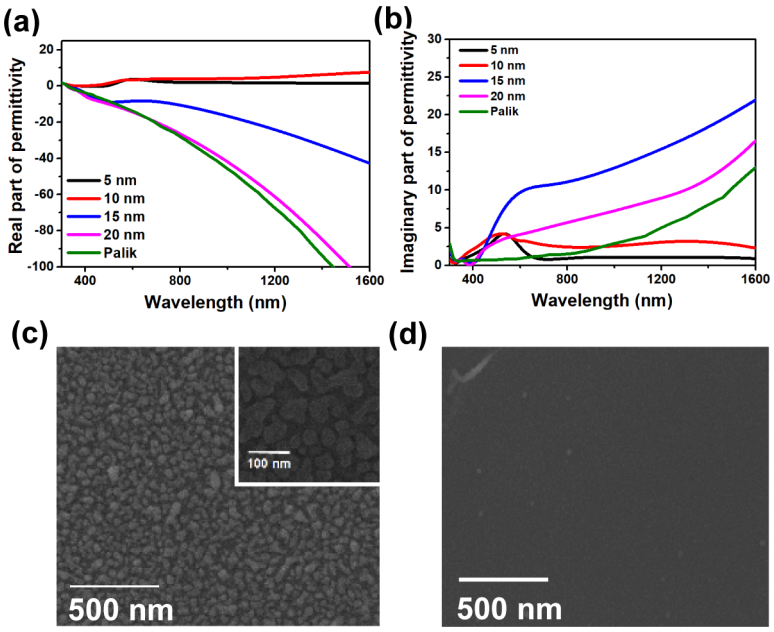

Fig. 1. (a) Real and (b) imaginary part of permittivity of silver thin films with different thicknesses. SEM images of silver thin film with thickness of (c) 10 and (d) 20 nm, respectively.

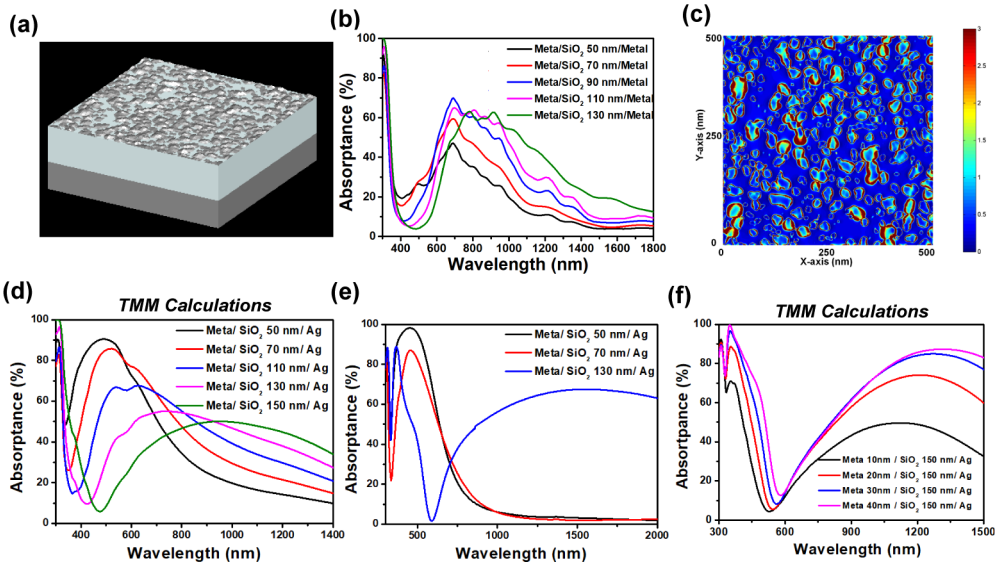

Fig. 2. (a) Schematic of a metasurface/SiO_2/silver absorber in the FDTD simulation domain. (b) FDTD predicted performance of absorbers with different spacer thicknesses. (c) Cross-sectional energy flow distributions of interaction between electromagnetic wave with silver metasurface at the incident wavelength of 750 nm. (d) TMM calculated and (e) measured absorption spectra of absorbers with different spacer layer thicknesses. (f) TMM calculated absorption spectra of absorbers with different metasurface thicknesses.

Optics EXPRESS

peak wavelength shifts toward longer wavelength, as shown in Fig. 2(d). To validate our TMM calculations, we fabricated and characterized the Metal/SiO_2/Metal absorbers with different SiO_2 spacer thickness. In general, the performance of the as-fabricated absorbers agrees with the absorptance spectra predicted by the TMM calculations, as indicated in Figs. 2(d)–2(e). However, the predicted absorptance peak wavelength does not match well with the measured value due to the assumption of particle-like metasurface as a smooth thin film in the TMM calculations

In addition to the 10 nm-thick metasurface coating, as discussed in Figs. 2(a)–2(e), we also investigate the effect of the metasurface coatings' thickness on absorption performance. Figure 2(f) shows that as the thickness of particle-like silver film is increased, the absorptance can be significantly enhanced. However, it is impossible to tune the thickness while maintaining the morphology of the coating by just controlling the magnetron sputtering parameters [42], such as deposition time, power, and argon pressure. This is inherent to the deposition process that yields continuous smooth film when the deposition thickness becomes sufficiently large. These thicker films differ from their thinner particle-like counterpart, as Fig. 1(c) and clearly demonstrated in Fig. 1(d).

In order to "unlock" this limitation of silver metasurface coating, while maintaining the effective optical properties caused by its particle-like morphology, we combine the sputtering deposition approach with graphene transfer coating, as shown in Fig. 3. To improve the graphene transfer coating, we carry out a pre-study of chemical vapor deposition (CVD) grown graphene transfer process on SiO_2/Si wafer, and we found that the backside surface of CVD-grown graphene on copper needs to be removed to minimize the defects and improve the monolayer graphene's uniformity, as discussed in Figs. 6(a)–6(b) of Appendix A. The schematic diagram of our layer-by-layer process is schematically shown in Fig. 3, which illustrates how graphene is transferred to silver amorphous metasurface. Details of the graphene transfer procedure are included in the experimental sections.

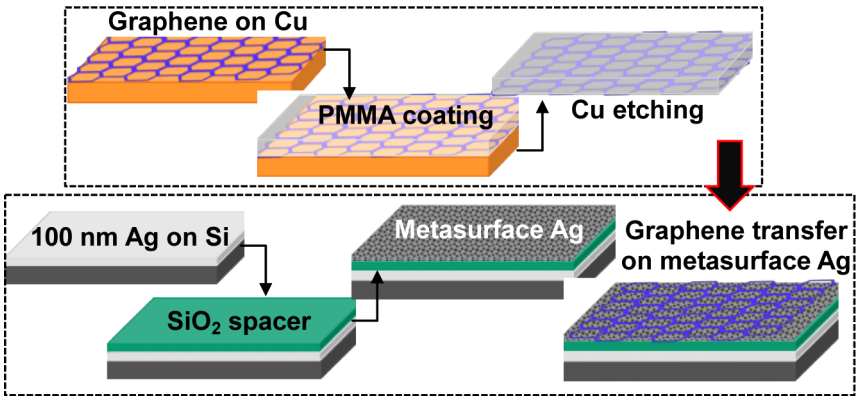

Fig. 3. Schematic of fabrications of silver (Ag) metasurface with tunable thickness by combing CVD-grown graphene transfer coating with thin film deposition using sputtering.

The integration of the graphene/silver metasurface absorber is carried out on a 100 nm-thick Ag layer that acts as a reflector and is deposited on a silicon wafer of 4 cm^2 in size. This is followed by deposition of a 130 nm SiO_2 film spacer by means of electron beam evaporation. On top of SiO_2, the 10 nm-thick silver metasurface is deposited using sputtering as previously explained. Thereafter, the monolayer CVD-grown graphene is transferred on the top of silver metasurface. The process is repeated and another 10 nm-thick silver metasurface is deposited on top of the graphene layer by sputtering. During the sequential coatings of the silver metasurface and monolayer graphene on SiO_2 coated silver reflector, SEM and UV-Vis

Optics EXPRESS

spectroscopy characterization are carried out to investigate the effect of each layer on the surface morphology and to assess the light absorption performance of as-fabricated samples.

SEM images show that once graphene is coated on the sample surface, the sputtered silver thin film exhibits denser particle-like morphology. This is due to the weak physical binding of graphene to the silver, and thus the silver deposition tends to form a more compact particle-like surface [43], as indicated by the comparison in Figs. 4(a)–4(b). A comparison between 10 nm-thick silver deposition on copper surface and graphene-coated copper surfaces also support the weak binding theory (between graphene and metal), as discussed in Figs. 8(a)–8(b) of Appendix C. Furthermore, Figs. 4(c)–4(d) shows that as the thickness of amorphous metasurface is increased, the performance of the as-fabricated absorbers exhibits a near-perfect absorption around 2 μm, which agrees with our predictions in Fig. 2(c). We also perform Fourier-transform infrared spectroscopy (FT-IR) characterization on our final device, which includes three-graphene transfers and four silver metasurface depositions, to investigate the overall absorptance performance in the mid-infrared regions. The as-fabricated multilayer metasurface/graphene integrated absorber exhibits near-unity absorptance around 1.9 μm with a broad bandwidth of 3.0 μm, as shown in Fig. 5(a). The demonstrated absorption structures in this work provide new design pathways in the realization of advanced graphene-based optoelectronic devices.

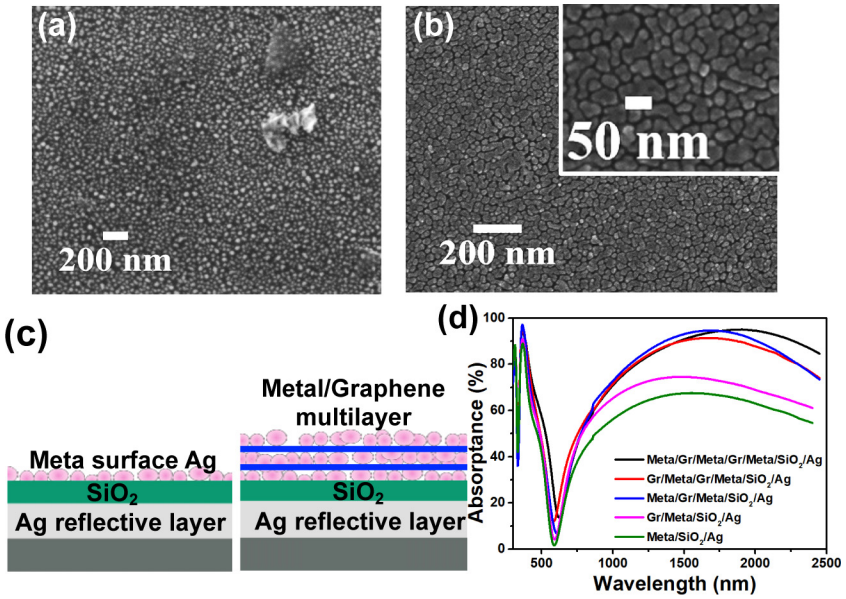

Fig. 4. (a-b) SEM images of silver metasurface on SiO_2 and graphene coated surface, respectively. (c) Schematic of multilayer of silver metasurface coating and graphene on SiO_2 coated Ag reflective layer. (d) Measured absorptance of integrated silver metasurface and graphene absorber.

In addition to the near-perfect light absorption performance of our proposed absorber, the silver amorphous metasurface coating has another foreseeable application: it enhances the Raman signals. We perform Raman characterization on metasurface/SiO_2/Ag, graphene/metasurface/SiO_2/Ag, and metasurface/graphene/ metasurface/SiO_2/Ag surfaces, as shown in Fig. 5(b). The Raman peak at 976 cm^{-1} is the characteristic response for the silver metasurface. For graphene, the typical Raman peaks are the defect (D) peak positioned at 1342 cm^{-1}, the G and 2D peaks that are at 1588 cm^{-1} and 2672 cm^{-1}, respectively. We found that as the graphene layer is sandwiched by two silver metasurfaces, the graphene Raman signal observed is extremely enhanced by the interaction between silver metasurfaces owing to the strong interaction of gap plasmon resonances

Optics EXPRESS

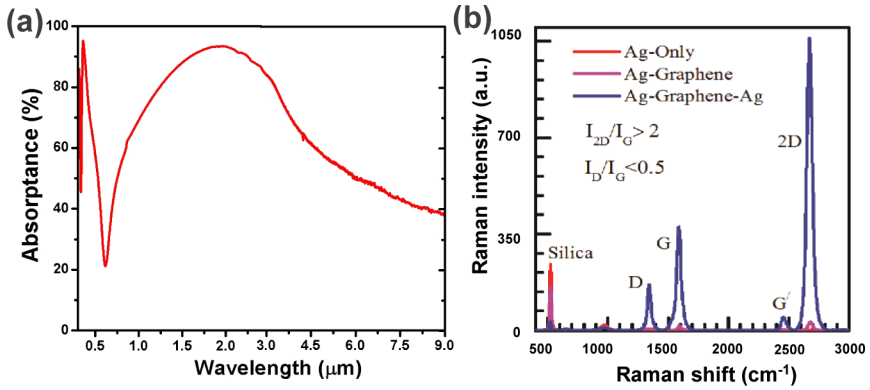

Fig. 5. (a) UV-Vis and FTIR measured absorptance of integrated silver metasurface with graphene absorber. (b) Raman characterization on silver metasurface, graphene coated silver metasurface, and graphene sandwiched by silver metasurfaces, respectively.

[44,45]. The enhancement caused by the sandwiched silver metasurface can be applied for surface enhanced Raman scattering applications [46,47].

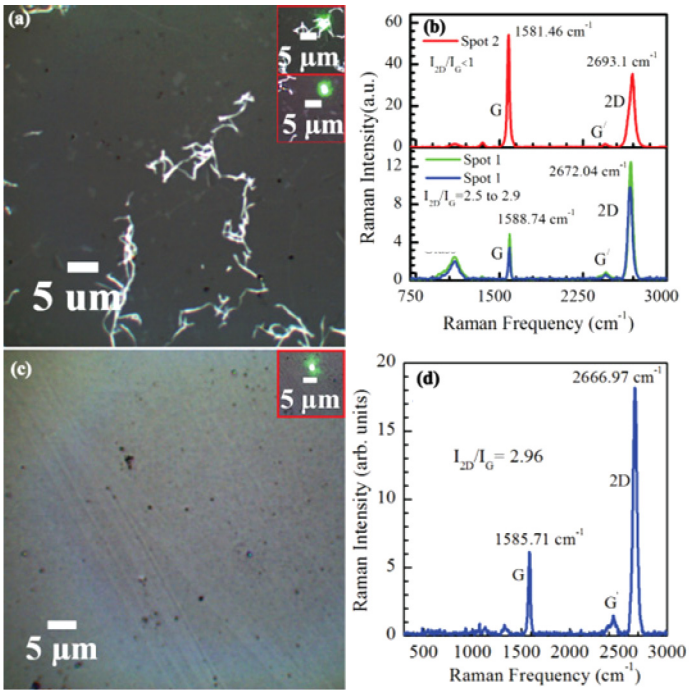

Fig. 6. Optical microscope images and Raman spectra of the transferred graphene layers SiO_2 without (a-b) and with (c-d) removing the backside graphene by using O_2 plasma treatment, respectively.

Optics EXPRESS

4. Conclusion

In summary, we proposed a facile approach consisting of a sputtering method with graphene transfer coating to design and fabricate thickness-tunable silver amorphous metasurface, which can achieve ultrathin broad light absorption over the near-infrared regions in a metasurface/insulator/metal configuration. Through SEM, and AFM characterization, we identified the particle-like morphology of the metasurface, which results in strong localized surface plasmon resonances. The proposed metasurface coatings have a variety of promising applications such as concentrated solar thermal power generation, photocatalysis, and surface-enhanced Raman scattering spectroscopies.

Appendix A: Uniform and clean transfer of CVD graphene coating

The procedure of achieving uniform and clean wet transfer of CVD graphene coating graphene transfer is introduced: first, Poly(methyl methacrylate) (PMMA) solution was spin-coated onto as-grown graphene samples at 2000 rpm for 90 seconds and then cured at 80°C for 3 mins. Here, a comparison of the graphene transferred SiO_2 surface with and without removing the backside graphene is shown in Fig. 6. We can find that an improved graphene transfer is achieved by removing the backside graphene on copper using oxygen plasma etching for 30 s where oxygen flow rate was 10 sccm prior to the etching copper using 2wt % aqueous ammonium persulphate solution. After graphene transferred to SiO_2/Silicon wafer, PMMA was removed with dilution in hot acetone (50°C). Without removing the backside graphene on copper surface, we found the defects on the transferred graphene surface, as shown in Figs. 6(a)–6(b) and non-uniform number of graphene layers, as indicated by the ratio of I(2D)/I(G) in the Raman spectra. By removing the backside graphene, the morphologies of the transferred monolayer graphene are more uniform and cleaner, as shown in Figs. 6(c)–6(d), which improve our graphene coating on silver metasurface.

Appendix B: Required optical constant for achieving near-perfect absorption

Using the transfer matrix method [41], we perform a quantitative analysis to evaluate the optical constants of the top layer on absorption performance. The optical absorber consists of a 10 nm-thick top layer, a silica spacer layer with 50 nm thickness in the middle, and a silver reflector at the bottom. For the incident wavelength of 500 nm, the absorptance is calculated with the different optical constants of the top layer, as shown in Figs. 7(a)-(b). The required optical constants of top layer are studied for different incident wavelengths ranging from 400 nm to 1500 nm, which shows similar trends of 10 nm- thick sputtered silver metasurface, as shown in Figs. 1(a)-(b).

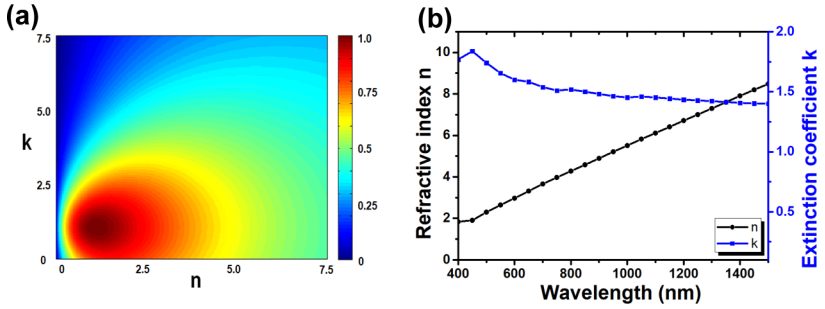

Fig. 7. (a) The dependence of optical constants of the top layer placed above the silica-coated metal surface on absorption performance (b) The required optical constant for achieving near perfect absorption with different incident wavelengths.

Optics EXPRESS

Appendix C: Surface morphologies of silver metasurface deposited on pure copper and graphene coated copper

We deposited 10 nm-thick silver thin film on pure copper foil and graphene coated copper surface fabricated by the chemical vapor deposition method. It can be observed that there is no particle-like morphology on the silver-deposited copper surface owing to strong binding between silver and copper. However, once the copper is coated by graphene, the silver particle-like metasurface is formed after the sputtering deposition owing to the weak binding between graphene and silver, as shown in Figs. 8(a)–8(b).

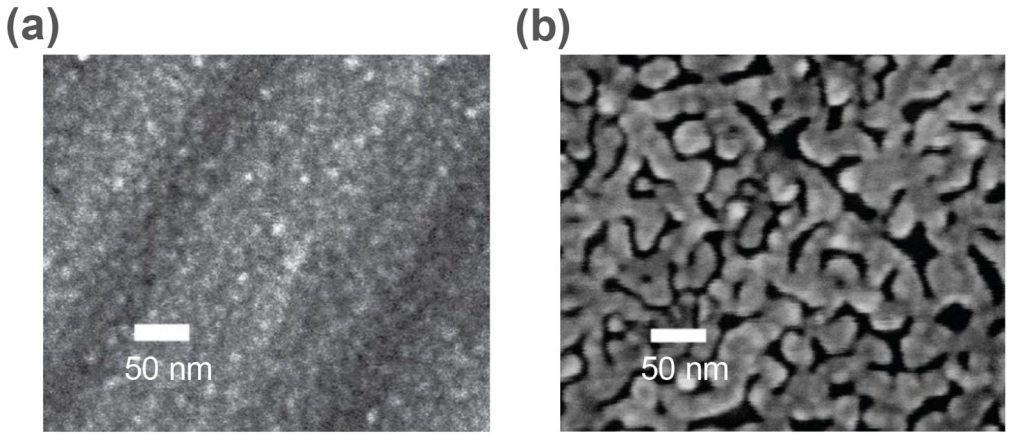

Fig. 8. SEM images of 10 nm-thick silver thin film deposited on (a) copper surface and (b) graphene coated copper surface.

Funding

Khalifa University of Science, Technology and Research (FR2017-000001); Universitetet i Tromsø (310059); Arctic Center for Sustainable Energy (ARC); Massachusetts Institute of Technology.

Acknowledgments

This work was funded under the Cooperative Agreement between the Khalifa University of Science and Technology, Masdar campus, Abu Dhabi, UAE and the Massachusetts Institute of Technology (MIT), Cambridge, MA, USA, Reference Number FR2017-000001. M.C. acknowledges the support of the Arctic Center for Sustainable Energy (ARC), UiT Arctic University of Norway through grant no. 310059.

References

1. D. Wu, C. Liu, Y. Liu, L. Yu, Z. Yu, L. Chen, R. Ma, and H. Ye, "Numerical study of an ultra-broadband near-perfect solar absorber in the visible and near-infrared region," Opt. Lett. **42**(3), 450–453 (2017).
2. A. Raza, J.-Y. Lu, S. Alzaim, H. Li, and T. Zhang, "Novel receiver-enhanced solar vapor generation: review and perspectives," Energies **11**(1), 253 (2018).
3. A. Tittl, A. U. Michel, M. Schäferling, X. Yin, B. Gholipour, L. Cui, M. Wuttig, T. Taubner, F. Neubrech, and H. Giessen, "A switchable mid-infrared plasmonic perfect absorber with multispectral thermal imaging capability," Adv. Mater. **27**, 4597–4603 (2015).
4. S. Molesky, C. J. Dewalt, and Z. Jacob, "High temperature epsilon-near-zero and epsilon-near-pole metamaterial emitters for thermophotovoltaics," Opt. Express **21**(S1), A96–A110 (2013).

Optics EXPRESS

5. N. Liu, M. Mesch, T. Weiss, M. Hentschel, and H. Giessen, "Infrared perfect absorber and its application as plasmonic sensor," Nano Lett. **10**(7), 2342–2348 (2010).
6. X.-F. Li, Y.-R. Chen, J. Miao, P. Zhou, Y.-X. Zheng, L.-Y. Chen, and Y.-P. Lee, "High solar absorption of a multilayered thin film structure," Opt. Express **15**(4), 1907–1912 (2007).
7. N. P. Sergeant, O. Pincon, M. Agrawal, and P. Peumans, "Design of wide-angle solar-selective absorbers using aperiodic metal-dielectric stacks," Opt. Express **17**(25), 22800–22812 (2009).
8. H. Hsiao, C. H. Chu, and D. P. Tsai, "Fundamentals and applications of metasurfaces," Small Methods **1**, 1600064 (2017).
9. G. M. Akselrod, J. Huang, T. B. Hoang, P. T. Bowen, L. Su, D. R. Smith, and M. H. Mikkelsen, "Large-Area Metasurface Perfect Absorbers from Visible to Near-Infrared," Adv. Mater. **27**(48), 8028–8034 (2015).
10. J. Tian, H. Luo, Q. Li, X. Pei, K. Du, and M. Qiu, "Near-Infrared Super-Absorbing All-Dielectric Metasurface Based on Single-Layer Germanium Nanostructures," Laser Photonics Rev. **12**, 1800076 (2018).
11. B. Zeng, Z. Huang, A. Singh, Y. Yao, A. K. Azad, A. D. Mohite, A. J. Taylor, D. R. Smith, and H.-T. Chen, "Hybrid graphene metasurfaces for high-speed mid-infrared light modulation and single-pixel imaging," Light: Sci. Appl. **7**(1), 51 (2018).
12. J. Toudert, R. Serna, M. G. Pardo, N. Ramos, R. J. Peláez, and B. Maté, "Mid-to-far infrared tunable perfect absorption by a sub-λ/100 nanofilm in a fractal phasor resonant cavity," Opt. Express **26**(26), 34043–34059 (2018).
13. Z. Zhou, K. Chen, J. Zhao, P. Chen, T. Jiang, B. Zhu, Y. Feng, and Y. Li, "Metasurface Salisbury screen: achieving ultra-wideband microwave absorption," Opt. Express **25**(24), 30241–30252 (2017).
14. R. C. Devlin, M. Khorasaninejad, W. T. Chen, J. Oh, and F. Capasso, "Broadband high-efficiency dielectric metasurfaces for the visible spectrum," Proc. Natl. Acad. Sci. **113**(38), 10473–10478 (2016).
15. Z. Zhang, J. Luo, M. Song, and H. Yu, "Large-area, broadband and high-efficiency near-infrared linear polarization manipulating metasurface fabricated by orthogonal interference lithography," Appl. Phys. Lett. **107**(24), 241904 (2015).
16. R. H. Siddique, J. Mertens, H. Hölscher, and S. Vignolini, "Scalable and controlled self-assembly of aluminum-based random plasmonic metasurfaces," Light: Sci. Appl. **6**(7), e17015 (2017).
17. A. K. Azad, W. J. M. Kort-Kamp, M. Sykora, N. R. Weisse-Bernstein, T. S. Luk, A. J. Taylor, D. A. R. Dalvit, and H.-T. Chen, "Metasurface broadband solar absorber," Sci. Rep. **6**(1), 20347 (2016).
18. M. J. Allen, V. C. Tung, and R. B. Kaner, "Honeycomb carbon: a review of graphene," Chem. Rev. **110**(1), 132–145 (2010).
19. Y.-C. Chiou, T. A. Olukan, M. A. Almahri, H. Apostoleris, C. H. Chiu, C.-Y. Lai, J.-Y. Lu, S. Santos, I. Almansouri, and M. Chiesa, "Direct Measurement of the Magnitude of the van der Waals Interaction of Single and Multilayer Graphene," Langmuir **34**(41), 12335–12343 (2018).
20. S. R. Tamalampudi, R. Sankar, H. Apostoleris, M. A. Almahri, B. Alfakes, A. Al-Hagri, R. Li, A. Gougam, I. Almansouri, M. Chiesa, and J.-Y. Lu, "Thickness-Dependent Resonant Raman and E′ Photoluminescence Spectra of Indium Selenide and Indium Selenide/Graphene Heterostructures," J. Phys. Chem. C **123**(24), 15345–15353 (2019).
21. P.-Y. Chen and A. Alù, "Terahertz metamaterial devices based on graphene nanostructures," IEEE Trans. Terahertz Sci. Technol. **3**(6), 748–756 (2013).
22. P.-Y. Chen, M. Farhat, and H. Bağcı, "Graphene metascreen for designing compact infrared absorbers with enhanced bandwidth," Nanotechnology **26**(16), 164002 (2015).
23. R. Alaee, M. Farhat, C. Rockstuhl, and F. Lederer, "A perfect absorber made of a graphene micro-ribbon metamaterial," Opt. Express **20**(27), 28017–28024 (2012).
24. D. Piccinotti, B. Gholipour, J. Yao, K. F. Macdonald, B. E. Hayden, and N. I. Zheludev, "Compositionally controlled plasmonics in amorphous semiconductor metasurfaces," Opt. Express **26**(16), 20861–20867 (2018).
25. A. G. Wattoo, R. Bagheri, X. Ding, B. Zheng, J. Liu, C. Xu, L. Yang, and Z. Song, "Template free growth of robustly stable nanophotonic structures: broadband light superabsorbers," J. Mater. Chem. C **6**(32), 8646–8662 (2018).
26. Y. Zhang, T. Wei, W. Dong, K. Zhang, Y. Sun, X. Chen, and N. Dai, "Vapor-deposited amorphous metamaterials as visible near-perfect absorbers with random non-prefabricated metal nanoparticles," Sci. Rep. **4**(1), 4850 (2014).
27. M. Choi, G. Kang, D. Shin, N. Barange, C.-W. Lee, D.-H. Ko, and K. Kim, "Lithography-free broadband ultrathin-film absorbers with gap-plasmon resonance for organic photovoltaics," ACS Appl. Mater. Interfaces **8**(20), 12997–13008 (2016).
28. J. Y. Lu, A. Raza, N. X. Fang, G. Chen, and T. Zhang, "Effective dielectric constants and spectral density analysis of plasmonic nanocomposites," J. Appl. Phys. **120**(16), 163103 (2016).
29. J. Y. Lu, A. Raza, S. Noorulla, A. S. Alketbi, N. X. Fang, G. Chen, and T. Zhang, "Near-Perfect Ultrathin Nanocomposite Absorber with Self-Formed Topping Plasmonic Nanoparticles," Adv. Opt. Mater. **5**(18), 1700222 (2017).
30. U. Schürmann, W. Hartung, H. Takele, V. Zaporojtchenko, and F. Faupel, "Controlled syntheses of Ag–polytetrafluoroethylene nanocomposite thin films by co-sputtering from two magnetron sources," Nanotechnology **16**(8), 1078–1082 (2005).
31. B.-T. Jheng, P.-T. Liu, and M.-C. Wu, "A promising sputtering route for dense Cu2ZnSnS4 absorber films and their photovoltaic performance," Sol. Energy Mater. Sol. Cells **128**, 275–282 (2014).
32. S. Andrikaki, K. Govatsi, S. N. Yannopoulos, G. A. Voyiatzis, and K. S. Andrikopoulos, "Thermal dewetting tunes surface enhanced resonance Raman scattering (SERRS) performance," RSC Adv. **8**(51), 29062–29070 (2018).

Optics EXPRESS

33. H. J. Yoon, Y. Jo, S. Jeong, J. W. Lim, and S.-Y. Lee, "Colored and semitransparent silver nanoparticle layers deposited by spin coating of silver nanoink," Appl. Phys. Express **11**(5), 52302 (2018).
34. J. W. Suk, A. Kitt, C. W. Magnuson, Y. Hao, S. Ahmed, J. An, A. K. Swan, B. B. Goldberg, and R. S. Ruoff, "Transfer of CVD-grown monolayer graphene onto arbitrary substrates," ACS Nano **5**(9), 6916–6924 (2011).
35. S. Shah, Y.-C. Chiou, C. Y. Lai, H. Apostoleris, M. M. Rahman, H. Younes, I. Almansouri, A. AlGhaferi, and M. Chiesa, "Impact of short duration, high-flow H2 annealing on graphene synthesis and surface morphology with high spatial resolution assessment of coverage," Carbon **125**, 318–326 (2017).
36. L. F. S. Http://www.lumerical.com, "Lumerical FDTD solutions," (n.d.).
37. J. Y. Lu and Y. H. Chang, "Implementation of an efficient dielectric function into the finite difference time domain method for simulating the coupling between localized surface plasmons of nanostructures," Superlattices Microstruct. **47**(1), 60–65 (2010).
38. E. D. Palik, *Handbook of Optical Constants of Solids* (Academic press, 1998), Vol. 3.
39. M. M. Rahman, H. Younes, J. Y. Lu, G. Ni, S. Yuan, N. X. Fang, T. Zhang, and A. AlGhaferi, "Broadband light absorption by silver nanoparticle decorated silica nanospheres," RSC Adv. **6**(109), 107951–107959 (2016).
40. M. M. Rahman, H. Younes, G. Ni, J. Y. Lu, A. Raza, T. J. Zhang, N. X. Fang, and A. A. Ghaferi, "Plasmonic nanofluids enhanced solar thermal transfer liquid," in *AIP Conference Proceedings* (2017), Vol. 1850.
41. C. C. Katsidis and D. I. Siapkas, "General transfer-matrix method for optical multilayer systems with coherent, partially coherent, and incoherent interference," Appl. Opt. **41**(19), 3978–3987 (2002).
42. D. Depla, S. Mahieu, and J. E. Greene, "Sputter deposition processes," in *Handbook of Deposition Technologies for Films and Coatings (Third Edition)* (Elsevier, 2010), pp. 253–296.
43. C. Gong, G. Lee, B. Shan, E. M. Vogel, R. M. Wallace, and K. Cho, "First-principles study of metal–graphene interfaces," J. Appl. Phys. **108**(12), 123711 (2010).
44. M. Schmelzeisen, Y. Zhao, M. Klapper, K. Müllen, and M. Kreiter, "Fluorescence enhancement from individual plasmonic gap resonances," ACS Nano **4**(6), 3309–3317 (2010).
45. Y. Li, Q. Li, C. Sun, S. Jin, Y. Park, T. Zhou, X. Wang, B. Zhao, W. Ruan, and Y. M. Jung, "Fabrication of novel compound SERS substrates composed of silver nanoparticles and porous gold nanoclusters: A study on enrichment detection of urea," Appl. Surf. Sci. **427**, 328–333 (2018).
46. W. Xu, X. Ling, J. Xiao, M. S. Dresselhaus, J. Kong, H. Xu, Z. Liu, and J. Zhang, "Surface enhanced Raman spectroscopy on a flat graphene surface," Proc. Natl. Acad. Sci. **109**(24), 9281–9286 (2012).
47. J.-Y. Lu, K.-P. Chiu, H.-Y. Chao, and Y.-H. Chang, "Multiple metallic-shell nanocylinders for surface-enhanced spectroscopes," Nanoscale Res. Lett. **6**(1), 173 (2011).